Low-Threshold Continuous-Wave 1.5-μm GaInNAsSb Lasers Grown on GaAs

Seth R. Bank, *Student Member, IEEE*, Mark A. Wistey, *Student Member, IEEE*, Lynford L. Goddard, Homan B. Yuen, Vincenzo Lordi, and James S. Harris, Jr., *Fellow, IEEE*

***Abstract*—We present the first continuous-wave (CW) edge-emitting lasers at 1.5 μm grown on GaAs by molecular beam epitaxy (MBE). These single quantum well (QW) devices show dramatic improvement in all areas of device performance as compared to previous reports. CW output powers as high as 140 mW (both facets) were obtained from 20 μm $\times$ 2450 μm ridge-waveguide lasers possessing a threshold current density of 1.06 kA/cm^2, external quantum efficiency of 31%, and characteristic temperature T_0 of 139 K from 10 °C–60 °C. The lasing wavelength shifted 0.58 nm/K, resulting in CW laser action at 1.52 μm at 70 °C. This is the first report of CW GaAs-based laser operation beyond 1.5 μm. Evidence of Auger recombination and intervalence band absorption was found over the range of operation and prevented CW operation above 70 °C. Maximum CW output power was limited by insufficient thermal heatsinking; however, devices with a highly reflective (HR) coating applied to one facet produced 707 mW of pulsed output power limited by the laser driver. Similar CW output powers are expected with more sophisticated packaging and further optimization of the gain region. It is expected that such lasers will find application in next-generation optical networks as pump lasers for Raman amplifiers or doped fiber amplifiers, and could displace InP-based lasers for applications from 1.2 to 1.6 μm.**

***Index Terms*—Auger recombination, continuous wave (CW), GaInNAs, GaInNAsSb, gallium arsenide, GaNAs, InGaAsN, intervalence band absorption, molecular beam epitaxy, optical communications, semiconductor laser, 1.5 μm, 1.55 μm.**

I. Introduction

KONDOW and coworkers [1], [2] discovered that the bandgap of GaNAs bows with the addition of nitrogen far more than conventional III-V alloys. Subsequent research has led to the realization of 1.3-μm GaInNAs lasers on GaAs. In the area of low-cost transmitters, the availability of lattice-matched AlAs–GaAs distributed Bragg reflector mirrors and lateral oxidation layers enable the fabrication of monolithic vertical-cavity surface-emitting lasers (VCSELs) [3]. To date, high performance 1.3-μm VCSELs have been reported using both molecular beam epitaxy (MBE) and metalorganic chemical vapor deposition (MOCVD) [4]–[6].

While GaAs-based lasers in the 1.5-μm range hold similar appeal for metro area network sources and pump lasers, the material challenges have been far more daunting. Wang and coworkers found that adding antimony as a surfactant during GaInNAs growth improved morphology and device performance, and allowed longer wavelength devices [7]. From $\boldsymbol{k}\cdot\boldsymbol{p}$ methods, it was theoretically predicted that nitride–antimonide alloys should possess similar bowing to the nitride–arsenides [8]. This was experimentally validated when it was found that cracked antimony incorporates into the crystal [9], [10], further redshifting emission and allowing the demonstration of lasers operating in pulsed mode out to 1.49 μm [11]. Refinement of these techniques, along with other improvements in growth technology, has allowed substantial improvements in device performance [12]–[14].

The remaining sections of this paper present GaInNAsSb materials characterization and edge-emitting device results. Section II describes the growth and materials characterization including photoluminescence (PL) and high-resolution X-ray diffraction (HR-XRD). Section III describes the device structure. As-cleaved measurements, including cavity length studies, are presented in Section IV. In Section V, progress toward high CW output powers is discussed. The results are analyzed to explain the limiting factors in the maximum CW output power and their implications for future device design.

II. Growth and Characterization

Single quantum-well (SQW) lasers were grown in two load-locked Varian Mod. Gen II solid-source MBE machines with nitrogen supplied by an SVT Associates Model 4.5 plasma cell. The cell was operated in a stable inductively coupled mode with 300 W of forward RF power and a nitrogen flow of 0.5 sccm. As discussed elsewhere [15], the nitrogen mole fraction was controlled directly with the group III growth rate rather than by varying the plasma conditions. The plasma source was ignited $\sim$20 min prior to active layer growth to allow the plasma to stabilize. Antimony was supplied with an unvalved cracking cell. The cracking region was held at 850 °C and the measured beam equivalent pressure was $\sim 1 \times 10^{-7}$ torr prior to growth. These conditions yielded almost entirely monomeric antimony and resulted in antimony mole fractions between 2% and 3%. Dimeric arsenic was supplied by a valved cracker and the group III sources with conventional effusion cells. Dopants

Manuscript received January 23, 2004; revised March 12, 2004. This work was supported in part by the Defence Advanced Research Projects Agency and Army Research Office under Contracts MDA972-00-1-024, DAAD17-02-C-0101 and DAAD199-02-1-0184, by the Office Naval Research under Contract N00014-01-1-00100, and in part by the Stanford Network Research Center (SNRC). The work of S. R. Bank, M. A. Wistey, and H. B. Yuen was supported by Stanford University fellowships. The work of L. L. Goddard was supported in part by a National Physical Science Consortium Fellowship and in part by the Xerox Palo Alto Research Center. The work of V. Lordi was supported by the Fannie and John Hertz Foundation.

The authors are with the Solid State and Photonics Laboratory, Stanford University, Stanford, CA 94305 USA (e-mail: sbank@stanford.edu).

Digital Object Identifier 10.1109/JQE.2004.828249

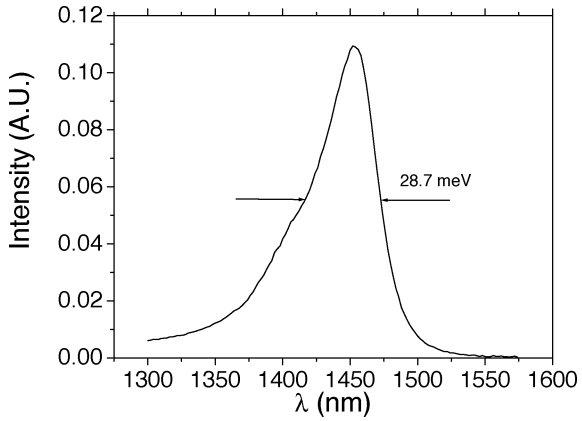

Fig. 1. Room-temperature PL spectrum of a single GaInNAsSb QW, with a linewidth of 28.7 meV.

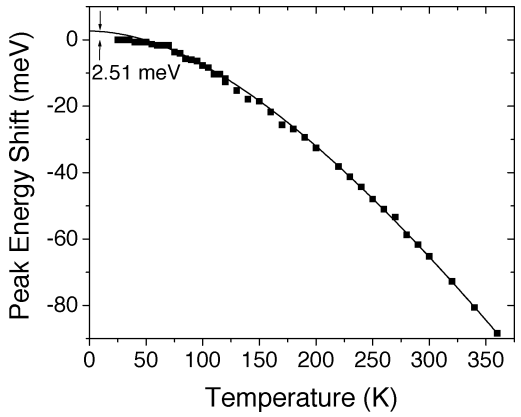

Fig. 2. Shift in the PL peak energy with temperature (squares) and the corresponding Varshni fit (line). The localization energy was found to be 2.5 meV.

were silicon and carbon, supplied by carbon tetrabromide. The growth chambers were kept under UHV (background pressure $\sim 10^{-10}$ torr) by a cryo-pump and an ion pump to minimize background impurities. GaAs substrates were cleaned at 350 °C for one hour in a separate chamber before introduction into the growth chamber. To remove the native oxide from the surface prior to buffer layer growth, the substrate was cleaned at 10 °C above the oxide desorption temperature ($\sim$ 580 °C) for 10 min under an arsenic overpressure. (Al)GaAs layers were grown at 20 °C above the oxide desorption temperature with 15× arsenic overpressure. GaNAs was also grown under a 15× overpressure but at $\sim$ 455 °C. The GaInNAsSb QW was grown under a 20× overpressure at 455 °C. These conditions have been found to produce the narrowest linewidth and highest intensity PL signal [13]. Similar to GaInNAs, the as-grown luminescence is rather poor and post-growth annealing is required to improve the radiative efficiency. The annealing behavior of GaInNAsSb is quite similar to that of GaInNAs and has been described in detail elsewhere [10], [11].

An example room-temperature PL spectrum, under a high excitation density of 10 kW/cm^2, is shown in Fig. 1. The linewidth was measured to be 28.7 meV with peak luminescence at 1.45 μm [13]. This sample was annealed at 800 °C for 1 min. This linewidth is comparable to those reported for the lowest threshold 1.2-μm InGaAs lasers [16] and 1.5-μm

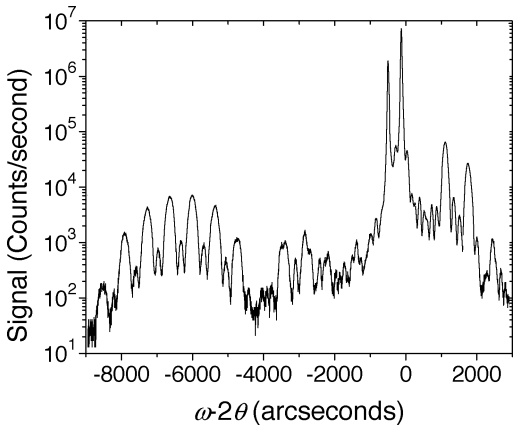

Fig. 3. HR-XRD ω-2θ scan of a triple QW sample. The visible oscillations indicate excellent epitaxial quality.

InGaAsP–InP lasers [17]. The peak signal is $\sim$9× higher than those reported in [11] and is due in part to improved growth technology [14], [18]. Additionally, temperature-dependent PL did not show the characteristic S-shaped curve seen in some GaInNAs samples, even for excitation densities as low as 5 W/cm^2 [19]–[21]. The S-shaped behavior has been attributed to band-tail states that arise from local potential fluctuations due to nonuniformities in the nitrogen distribution [19]. These fluctuations provide confinement for excitons at reduced temperatures. The S-shape arises as the emission changes from mainly due to localized excitons (low temperatures) to that of a pure band-to-band transition (high temperatures). The degree of localization has been directly linked to material quality, specifically the presence of nonradiative centers [19], [21]. Even when no S-shape is observed, there still exists a significant difference between the measured data and the best Varshni fit at low temperatures (<75 K) [22]. This energy difference, termed the localization energy, is directly related to the nitrogen content and inversely related to the material quality. The shift in the PL peak with temperature for the GaInNAsSb QW of Fig. 1 is shown in Fig. 2. While no S-shaped curve is observed in our samples at low temperatures, a localization energy of 2.5 meV was required to properly fit to the Varshni model. This is, however, more than two times lower than the localization energies reported in [22] for GaInNAs films of comparable nitrogen content. This is further evidence of enhanced crystal quality due to the addition of antimony and improvements in growth techniques. Additionally, GaInNAs QWs grown under similar conditions to those in Fig. 1, but with PL peak around 1.3 μm, show similar behavior. This evidence suggests that while some degree of localization remains, the addition of antimony and refined growth techniques have improved material homogeneity significantly.

An HR-XRD ω-2θ scan of a nominally identical triple QW sample is shown in Fig. 3. The narrow and well-resolved Pendellosung fringes indicate excellent epitaxial quality. A (224) reciprocal space map is also shown in Fig. 4. No relaxation or phase segregation is evident from the figure, which shows all diffraction resulting from the same in-plane lattice parameter. Any relaxation of the compressively strained QW would result in a diffraction peak located to the lower left of the substrate

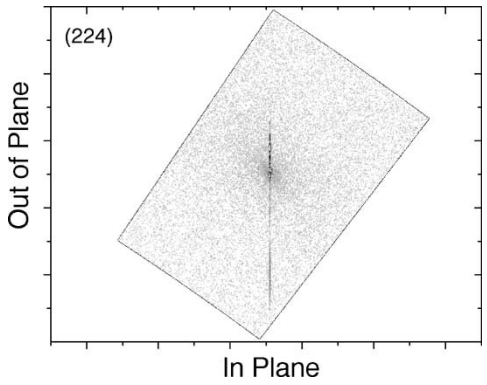

Fig. 4. (224) reciprocal space map showing no evidence of relaxation or phase segregation.

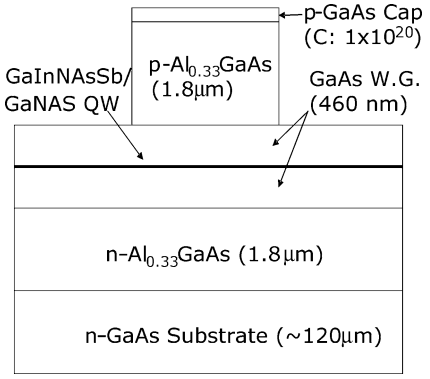

Fig. 5. Schematic view of the edge-emitting device structure used for this study.

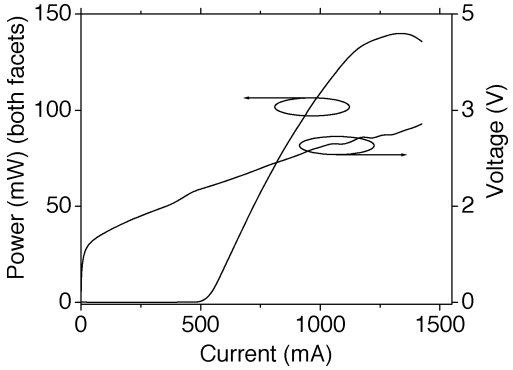

Fig. 6. CW $L-I-V$ of a $20\,\mu\text{m} \times 2450\,\mu\text{m}$ device.

diffraction peak, while relaxation of the tensile barriers would be found in a peak located to the upper right of the substrate peak. However, no additional peaks are present.

III. Device Structure

The lasers used in this study were of the separate confinement heterostructure ridge-waveguide type. A schematic diagram of the device structure is shown in Fig. 5. The active layer was a single 75-Å $Ga_{0.62}In_{0.38}N_{0.023}As_{0.95}Sb_{0.027}$ quantum well surrounded on either side by 220-Å $GaN_{0.025}As_{0.975}$ barriers. Compositions were determined through prior measurements of similar structures using a combination of HR-XRD, Rutherford backscattering, and nuclear reaction analysis [23]. GaNAs barriers exhibit improved low-temperature growth morphology, as compared to GaNAsSb, while also providing strain compensation [18]. It is important to note that this has only been examined over the narrow window of barrier growth conditions dictated by these QW compositions. Work is currently underway to investigate this further. Moreover, the removal of antimony from the barriers may provide superior hole confinement due to a larger valence band offset between the QW and barrier. Some additional improvement in PL linewidth is likely due to diminished alloy disorder.

The active layer was symmetrically embedded in a GaAs waveguide with a total thickness of ~ 4600 Å. A thickness of one optical wave was chosen to approximately maximize the overlap between the optical field and the quantum well. The n-type cladding of the laser was 1.8 μm of $Al_{0.33}Ga_{0.67}As$ with the outer 9000 Å doped at 3×10^{18} cm^{-3} and the inner 9000 Å doped at 7×10^{17} cm^{-3}. The p-type cladding was a similar structure, with the inner 9000 Å doped at 5×10^{17} cm^{-3} and the outer 9000 Å was doped at 3×10^{18} cm^{-3}. The regions nearest to the core were doped more lightly to minimize free carrier absorption (FCA) losses. A 500-Å top p-type GaAs cap layer was doped at $\sim 1 \times 10^{20}$ cm^{-3} to facilitate low-resistance ohmic contacts.

The sample was *ex situ* annealed at 800 °C for one min in a rapid thermal annealing furnace where arsenic outdiffusion was minimized with a GaAs proximity cap. Ridge widths of 5, 10, and 20 μm were defined using a combination of lift-off of evaporated Ti–Pt–Au and a self-aligned dry etch to the top of the GaAs waveguide. The wafer was then thinned to $\sim 120\,\mu$m and backside metal (Au–Ge–Ni–Au) was evaporated. To reduce contact resistance, the structure was sintered at 410 °C for one min. Fabry–Perot cavities of multiple lengths were defined by cleaving.

IV. As-Cleaved Devices

A. Room-Temperature Measurements

Testing was performed epitaxial-side up on a temperature-controlled copper heatsink. Unless otherwise specified, all parameters were measured at room temperature (20 °C), under CW operation, on as-cleaved facets. Fig. 6 shows the light output and voltage versus current input ($L-I-V$) curves for a 20 μm $\times$ 2450 μm device. The threshold current density J_{th} was measured to be 1.06 kA/cm^2. Lasing occurred at 1.498 μm as shown in Fig. 7. The slope efficiency above threshold was 0.26 W/A corresponding to an external quantum efficiency η_e of 31%. Efficiencies as high as 40% were observed in shorter devices. These low values are attributed to carrier leakage from the well and also poor material quality of the barriers. These effects will be discussed in more detail elsewhere [24]. The peak output power at thermal rollover was 140 mW from both facets. From Fig. 6, the diode turn-on voltage was low, $\sim$1.0 V, and the peak voltage was $\sim$3 V, indicating such devices could be driven directly by CMOS. The ideality and series resistance were rather high, $\sim$3 and 1.3 Ω, respectively. The relatively high series resistance is likely caused by the thin p-side contact and, to some extent, the low doping in the cladding layers to minimize FCA. Approximately 50% of the 4000 Å of gold,

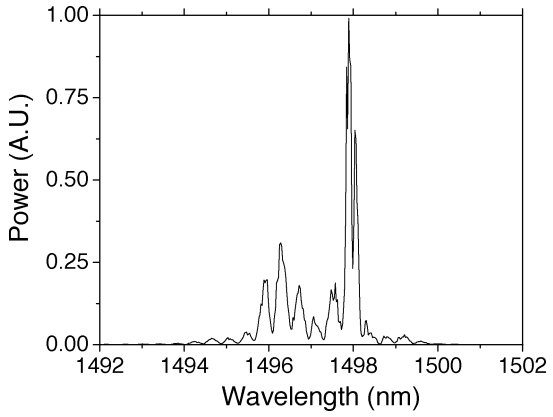

Fig. 7. Lasing spectrum of the $20\ \mu\text{m} \times 2450\ \mu\text{m}$ device showing oscillation at 1.498 μm.

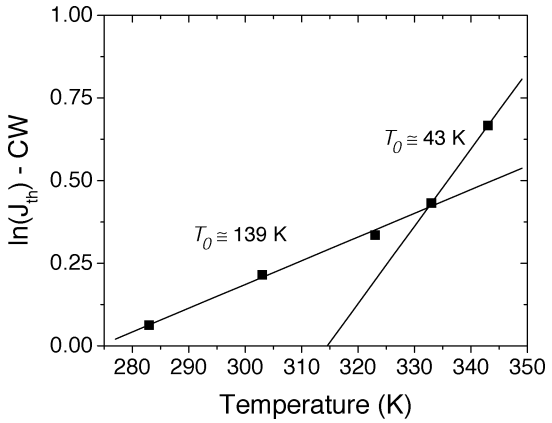

Fig. 8. Plot of CW $\ln(J_{\text{th}})$ with temperature (squares) and the fits to an Arrhenius relation (lines) for a $20\ \mu\text{m} \times 2450\ \mu\text{m}$ device. The T_0 value for each temperature range is indicated.

on the top contact, was removed during the dry etch which resulted in substantial spreading resistance, ohmic heating, and possibly nonuniform carrier injection along the length of the device. Devices were probed at several points along the length of the ridge to compensate for this effect.

B. Temperature Dependence

The effects of device temperature were also explored. The natural logarithm of the threshold current density and peak output power are plotted with heatsink temperature in Fig. 8. The characteristic temperature T_0 was found to be 139 K measured over the range of temperatures from 10 °C–60 °C and 43 K from 60 °C–70 °C. This sharp kink in the $J_{\text{th}}(T)$ curve is due to the rapid onset of Auger processes, which scale with the cube of the carrier density, and strongly increase the temperature sensitivity. Moreover, CW lasing was not observed above 70 °C. The loss of laser action is attributed to the onset of Auger recombination and may also be correlated with carrier leakage [24], [25]. From spontaneous emission (z-parameter) measurements performed on these lasers, Auger recombination is found to dominate laser operation when the current density rises above $\sim$1.5–2 kA/cm^2, in agreement with Fig. 8 [25]. The z-parameter technique has shown similar evidence of Auger recombination in 1.3-μm GaInNAs lasers [26]. Moreover, the kink in $J_{\text{th}}(T)$ was always observed at the temperature where J_{th} reached $\sim$1.5–2 kA/cm^2, regardless of device length. As will be shown in the next section, this appears to be a commonality among all GaInNAs(Sb) devices reported in this wavelength regime. Onset of Auger recombination was also found to be independent of temperature over the range studied, indicating a low activation energy of Auger processes, $E_a \leq 27$ eV [24], [25], [27].

The wavelength shift with temperature was measured to be 0.58 nm/K, or 0.32 meV/K. This agrees with the shift observed for GaInNAs-based lasers at 1.3 μm [28] and is similar to that of InGaAsP lasers at 1.5 μm [29]. Due to this temperature dependence, CW laser action was observed at 1.52 μm at a heatsink temperature of 70 °C. This is the first report of CW GaAs-based laser operation at 1.5 μm and beyond.

C. Comparison of QW and Barrier Designs

Through comparison with other published dilute nitride lasers, it is now possible, to some extent, to evaluate the effects of QW and barrier material design on device performance. We conclude from the analysis that Auger recombination is significant in all the approaches at wavelengths $\sim$ 1.5 μm. Additionally, GaNAs may have a weak type-II band lineup with GaAs.

Several different approaches have been reported in the literature to reach 1.5 μm including GaInNAs with GaAs barriers (termed GaInNAs–GaAs) [30] and GaInNAsSb with GaNAsSb barriers (GaInNAsSb–GaNAsSb) [12]. It is noted that the lasers reported here (GaInNAsSb–GaNAs) have both a reduced J_{th} and higher T_0 than the approaches in [12] and [30]. As a result, we can conclude that any improvement in T_0 reported here is due to improved device structure and not simply an artifact of temperature insensitive nonradiative centers. We may similarly rule out Auger recombination as the cause for reduced room temperature T_0; spontaneous emission measurements show that Auger recombination only becomes significant when the threshold current density is elevated above $\sim$ 1.5–2 kA/cm^2 (i.e., those necessary at higher temperatures) [25]. Each reported laser structure shows a kink in $J_{\text{th}}(T)$ at a current density of $\sim$2–4 kA/cm^2-per-well, similar to that in Fig. 8 [12], [30]. Additionally, the T_0 above this point is similar in each case: 69 K in [30], 68 K in [12] (estimated from figure), and 43 K here. The 43 K reported here is smaller than the others; we believe this may be due to error extracting T_0 from only two data points (Fig. 8). It should be noted that Auger recombination is not the dominant loss mechanism *at room temperature*, but it does dominate at elevated threshold current densities. Based upon the preceding discussion, Auger recombination appears to be a universal characteristic of the nitride–arsenide alloys reported thus far beyond $\sim$ 1.4 μm. Neither changes in barrier material nor presence of antimony have mitigated these effects to date. In pushing to 1.55 μm, the choice of additional indium or antimony to redshift the alloy will likely be determined by the Auger coefficient of the resulting quantum wells.

The dominant mechanism affecting T_0 at low temperatures, in the lasers reported here, is likely carrier leakage, possibly of holes, from the QW due to weak valence band confinement [16]. This is likely also the case for 1.3-μm GaInNAs–GaAs lasers [31]. In light of the improvements in T_0 reported here (139 K compared to 111 K), we conclude that the addition of nitrogen into the barriers increases the QW valence band offset which leads to the conclusion of type-II confinement. This observation is in agreement with band-offset measurements and laser studies by Tansu *et al.* at shorter wavelengths [31]. Tansu and coworkers found a simultaneous reduction in $J_{\rm th}$ and enhancement in T_0 when they changed from GaAs to GaNAs barriers surrounding a GaInNAs QW. They attributed this improvement to a reduction in hole leakage due to the increased valence band offset between the QW and barrier due to the type-II nature of GaNAs–GaAs. It is, however, difficult to determine whether the difference in valence band offset, in the case of $\sim$ 1.5 μm lasers, is due to the presence of nitrogen in the barriers or is simply due to the presence of antimony in the QW. Band-offset measurements of GaAsSb with GaAs show that bandgap reduction takes place primarily in the valence band up to $\sim$40% antimony [32]. The improvement in T_0 reported here may also be due to the reduced carrier density in the QW from reduced nonradiative recombination and higher material gain. This could reduce carrier overflow into the confinement regions, thereby increasing T_0 [33].

Similarly, a T_0 of 83 K was reported in [12] for GaInNAsSb–GaNAsSb devices. While the difference in T_0 may also be due to reduced threshold carrier density, the valence band offset is reduced through the addition of antimony into the barriers. This is further compounded by the growth morphology problems of GaNAsSb grown at low temperatures [18]. We conclude, therefore, that GaNAs is likely a superior barrier material for 1.5-μm lasers. Moreover, increasing the antimony content in the QW would further improve hole confinement, thereby increasing both T_0 and η_i.

D. Cavity Length Studies

Cavity length studies of $J_{\rm th}$ and η_e, in pulsed mode, were employed to determine various device parameters. The results of the cavity length study are summarized for each stripe width in Table I. Fig. 9 plots $1/\eta_e$ as a function of cavity length, L, for 10-μm-wide stripes. The linearity of $1/\eta_e$ with L insures that parameters extracted were not influenced by effects that become significant at short cavity lengths [34]. The internal loss was found to be quite low, in the range of 1.91–4.7 cm^{-1} for 5, 10, and 20 μm stripes [35]. The loss for 5-μm wide stripes, 1.91 cm^{-1}, is comparable to some of the best results for InP waveguides [36] and is lower than 1.5-μm InAs quantum-dot lasers grown on GaAs [37]. The internal quantum efficiency, η_i, was found to be between 42% and 50%. This low value may be due to short carrier residency in the QW in conjunction with nonradiative centers within the GaNAs barriers. While GaNAs barriers are of superior optical quality to GaNAsSb, under these growth conditions, they likely possess large numbers of nonradiative centers. An additional mechanism for the low η_i may be poor interfaces between the QW and barriers, however, no evidence currently supports such a mechanism. More work is needed to identify and remedy the cause(s) for the low η_i.

TABLE I
SUMMARY OF CAVITYLENGTH STUDY

Parameter	5 µm Stripe	10 µm Stripe	20 µm Stripe
η_i (%)	42	49	46
α_i (cm^{-1})	1.91	4.69	3.00
Γ-g_0(cm^{-1})	25.0	25.7	26.2
g_0(cm^{-1})	1786	1836	1871
J_{tr}(A/cm^2)	635	658	479
β_0(cm/A)	2.81	2.79	3.91
R_{th}(K/W) (L = 983 µm)	41.5	37.8	30.8

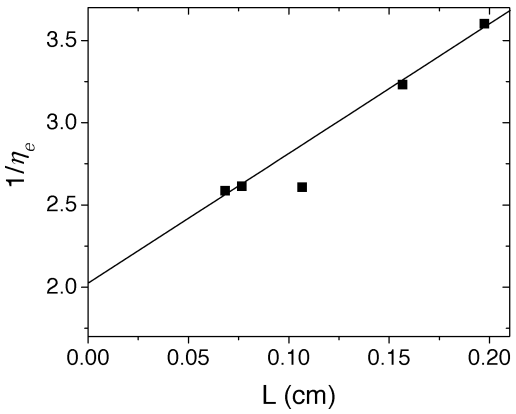

Fig. 9. Plot of $1/\eta_e$ with cavity length (squares) and the fit to theory (line) for 10-μm-wide lasers, measured under pulsed operation.

As shown in Fig. 10, the internal loss α_i was found to be moderately temperature dependent. The characteristic temperature of α_i was $\sim$306 K when fitted to an Arrhenius relation. This is likely due to parasitic intervalence band absorption (IVBA) and is a significant loss mechanism in these lasers. Theoretical and experimental studies have found IVBA to be, in general, strongly temperature dependent in unstrained InGaAs–InP devices in the range of interest [38], [39]. For GaAs, IVBA is expected to have a characteristic temperature of $\sim$300 K, which agrees with the measured internal loss data of Fig. 10 [38]. The small values of $\alpha_i(T)$ indicate that while IVBA processes are significant, they are not currently the dominant loss mechanisms. Removal of this process would only increase T_0 by $\sim$5 K. Some fraction of α_i is also likely due to waveguide roughness and other unavoidable loss mechanisms. To quantify this somewhat, these losses may be estimated by extrapolating α_i

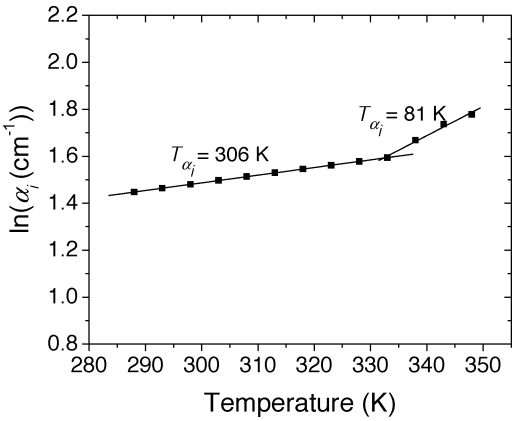

Fig. 10. Measured $\ln(\alpha_i)$ for 20 μm stripes as a function of device temperature (squares) extracted under pulsed (1 μs, 1% duty cycle) operation to minimize device heating. Fits to experimental data are also shown (line). The increase in loss with temperature is a strong indication of IVBA.

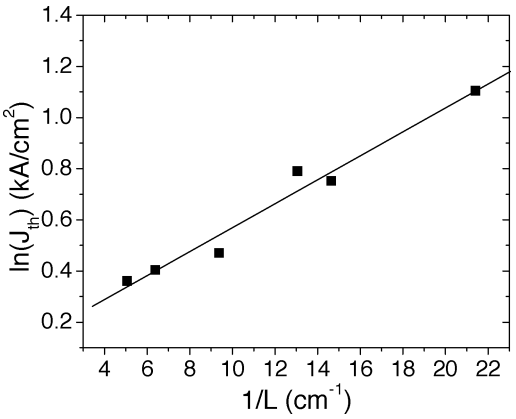

Fig. 11. Plot of $\ln(J_{\rm th})$ with the inverse of cavity length (squares) and fit to theory (line) for 10-μm-wide lasers, measured under pulsed operation.

to 0 K, yielding 0.51 cm^{-1}. Removing this extrapolated loss, the characteristic temperature for the internal loss was 273 K. Above $\sim$ 60 °C, there is a kink in the $\alpha_i(T)$ curve that is attributed to the turn-on of Auger recombination, in concert with incomplete Fermi level pinning along the device length. This is an artifact of the device structure caused by the thin p-type ohmic contact. Some devices showed sensitivity to Auger recombination in $\eta_e(T)$ and others did not.

A plot of $\ln(J_{\rm th})$, with $1/L$, for 10-μm stripes is shown in Fig. 11. Using conventional methods [40], the gain overlap product $\Gamma \cdot g_0$ was determined to be $\sim$25–26 cm^{-1} and the transparency current density J_{tr} was found to be $\sim$0.5–0.65 kA/cm^2. From finite difference simulations, a two-dimensional overlap of the fundamental mode with the active region $\Gamma = 1.4\%$ was calculated, yielding a gain coefficient, g_0, in the range 1786–1871 cm^{-1}. This is higher than for GaInNAs–GaNAs lasers at 1.3 μm [31] and InGaAsP lasers at 1.5 μm [17], [41]. With continued improvements in η_i and J_{tr}, GaInNAsSb will become quite promising for high power laser applications, including Raman pump lasers.

Based on these data, the peak differential gain at transparency, $\beta_0 = g_0/J_{tr}$, was quite low, 2.79–3.91 cm/A, and predicts poor current modulation response. This is attributed mainly to the large number of nonradiative recombination sites and improved

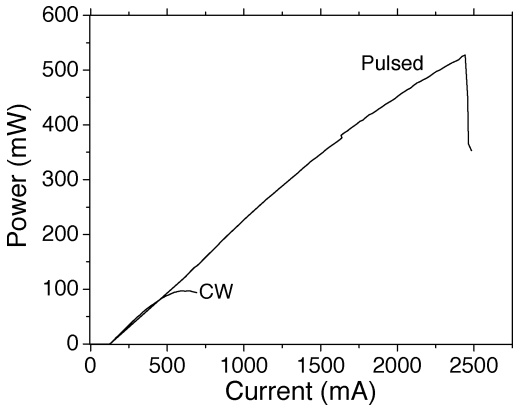

Fig. 12. $L - I$ curves under pulsed and CW operation for an HR coated 10 μm $\times$ 983 μm laser. Peak output power was limited by COD under pulsed excitation and thermal rollover under CW operation.

results are expected through advances in growth techniques. It is also expected that the actual differential gain with respect to carrier density, dg/dn, will be significantly higher than predicted by β_0 due to the low η_i and J_{tr}.

V. High-Power Lasers

In an attempt to obtain higher output powers, a highly reflective coating ($\sim$98.7%) was applied to one facet and the other was left as-cleaved. The best $J_{\rm th}$ and η_e obtained were 1.05 kA/cm^2 and 44%, respectively. Fig. 12 shows representative $L-I$ curves for 10 μm $\times$ 983 μm devices under pulsed (1 μs, 1% duty cycle) and CW operation. The single facet CW output power and efficiency are approximately the same as that observed from both facets of uncoated devices with the same mirror loss.

Under pulsed conditions, the peak output power was substantially higher than under CW operation, 527 mW versus 100 mW. The difference in output power is attributed to the high thermal resistance associated with mounting devices epitaxial-side up during testing. Measurements of the thermal resistance show it to be $\sim$38 K/W for a 10 μm $\times$ 983 μm device, which agrees with theory [42]. Calculations indicate a threefold to fourfold reduction in CW device heating if devices are mounted epitaxial-side down. Moreover, the sharp decrease of the peak CW output power with chuck temperature (Fig. 13) indicates that ohmic heating and the temperature sensitivity of threshold and efficiency are important issues for achieving high CW output power. Over the limited temperature range of the measurements, the electrical and thermal resistivities of the semiconductor layers increase approximately linearly [43], [44]. This is in agreement with the observations of Fig. 13, when the variations in α_i and $J_{\rm th}$ are considered. Additionally, higher pulsed output powers, up to 707 mW, were observed from the 20 μm $\times$ 1000 μm device shown in Fig. 14. If thermal management is improved, CW output powers $\sim$500 mW are considered feasible from a SQW laser with minimal added packaging and processing.

The rapid degradation in pulsed output power shown in Fig. 12 is attributed to catastrophic optical mirror damage (COD) and/or burnout of the p-side contact directly under the probe tip. The optical power density was calculated to be $\sim$ 4.9 MW/cm^2 at the onset of failure, which is in agreement

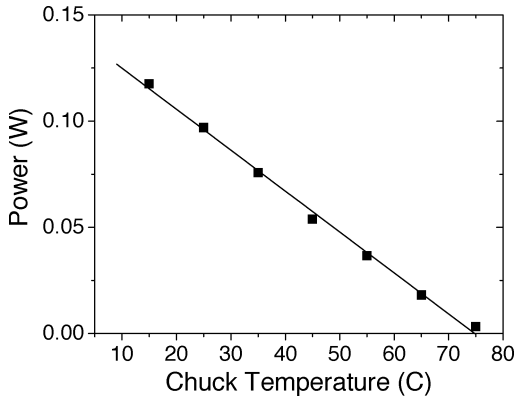

Fig. 13. Peak CW output power for an HR coated $10\ \mu\text{m} \times 983\ \mu\text{m}$ laser as a function of ambient temperature (squares) and a linear fit (line). The increase in threshold and decrease in gain with temperature, along with slight increases in thermal and electrical resistance, produce a nearly linear relationship between peak CW output power and chuck temperature.

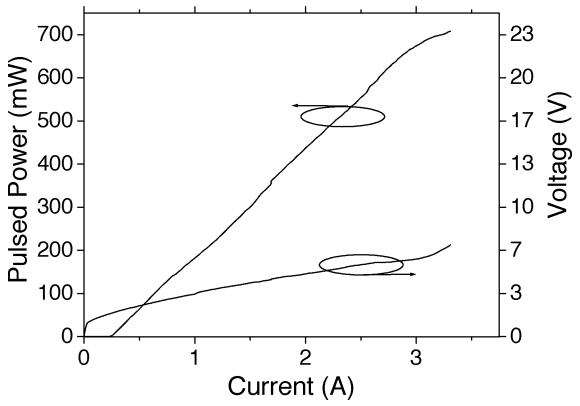

Fig. 14. Pulsed $L - I$ curve for a $20\ \mu\text{m} \times 1000\ \mu\text{m}$ HR coated device. A peak output power of 707 mW, limited by the laser driver, was achieved from the uncoated facet.

with the 1–5 MW/cm^2 COD threshold generally observed for as-cleaved AlGaAs–GaAs laser facets [45]. As discussed earlier, the p-side contact was rather thin after the self-aligned etch and ~30% of the ohmic heating in the device occurred along the contact. This parasitic heating mechanism can be eliminated without substantially more complex processing.

VI. Conclusion

We have demonstrated low-threshold CW 1.5-μm lasers grown on GaAs using GaInNAsSb–GaNAs as the active layer. A 20 μm $\times$ 2450 μm SQW ridge-waveguide device showed both high output power, ~140 mW, and T_0 of 139 K. Both values represent a substantial improvement over previously reported GaInNAs(Sb) devices beyond 1.3 μm. The reduced J_{th}, 1.06 kA/cm^2, and higher T_0 validate the recent improvements in growth technology. These devices lased CW at 1.498 and 1.52 μm at room temperature and 70 °C, respectively. From cavity length studies, a high $g_0, \sim 1800\ \text{cm}^{-1}$, was found and is promising for future high power laser applications. Progress toward high-power edge-emitting lasers was also demonstrated, including 707 mW of pulsed output power from a single facet. The peak output power was limited by COD under pulsed conditions and thermal rollover during CW operation. By mounting devices epi-side down, much higher CW powers are expected. If improvements in the active region follow the trend of GaInNAs at 1.3 μm, GaInNAsSb devices will become quite promising for next-generation optical networks.

Acknowledgment

The authors would like to thank Prof. A. R. Adams at the University of Surrey for discussions regarding Auger recombination and IVBA. They also wish to thank S. Zou of Santur Corp. for assistance in wafer thinning and facet coatings and A. Moto of Sumitomo Electric Industries for helpful discussions and donation of substrates. W. Ha of Novalux, V. Gambin of Lockheed Martin, and V. Sabnis of Stanford University also provided many useful insights.

References

[1] M. Kondow, K. Uomi, A. Niwa, T. Kitatani, S. Watahiki, and Y. Yazawa, "GaInNAs: A novel material for long-wavelength-range laser diodes with excellent high-temperature performance," *Jpn. J. Appl. Phys.*, vol. 35, pp. 1273–1275, Feb. 1996.

[2] M. Kondow, T. Kitatani, S. Nakatsuka, M. C. Larson, K. Nakahara, Y. Yazawa, M. Okai, and K. Uomi, "GaInNAs: A novel material for long-wavelength semiconductor lasers," *IEEE J. Select. Topics Quantum Electron.*, vol. 3, pp. 719–730, June 1997.

[3] C. W. Coldren, M. C. Larson, S. G. Spruytte, and J. S. Harris, "1200 nm GaAs-based vertical cavity lasers employing GaInNAs multiquantum well active regions," *Electron. Lett.*, vol. 36, pp. 951–952, May 2000.

[4] K. D. Choquette, J. F. Klem, A. J. Fischer, O. Blum, A. A. Allerman, I. J. Friz, S. R. Kurz, W. B. Breiland, R. Sieg, K. M. Geib, J. W. Scott, and R. L. Naone, "Room temperature continuous wave InGaAsN quantum well vertical-cavity lasers emitting at 1.3 μm," *Electron. Lett.*, vol. 36, pp. 1388–1390, Aug. 2000.

[5] G. Steinle, H. Riechert, and A. Y. Egorov, "Monolithic VCSEL with InGaAsN active region emitting at 1.28 μm and CW output power exceeding 500 μW at room temperature," *Electron. Lett.*, vol. 37, pp. 93–95, Jan. 2001.

[6] T. Takeuchi, Y. L. Chang, M. Leary, A. Tandon, H. C. Luan, D. Bour, S. Corzine, R. Twist, and M. Tan, "1.3 μm InGaAsN vertical cavity surface emitting lasers grown by MOCVD," *Electron. Lett.*, vol. 38, pp. 1438–1440, Nov. 2002.

[7] X. Yang, M. J. Jurkovic, J. B. Heroux, and W. I. Wang, "Molecular beam epitaxial growth of InGaAsN:Sb/GaAs quantum wells for long-wavelength semiconductor lasers," *Appl. Phys. Lett.*, vol. 75, pp. 178–180, July 1999.

[8] B. N. Murdin, A. R. Adams, P. Murzyn, C. R. Pidgeon, I. V. Bradley, J. P. R. Wells, Y. H. Matsuda, N. Miura, T. Burke, and A. D. Johnson, "Band anticrossing in dilute InN_xSb_{1-x}," *Appl. Phys. Lett.*, vol. 81, pp. 256–258, July 2002.

[9] H. Shimizu, K. Kumada, S. Uchiyama, and A. Kasukawa, "High performance CW 1.26 μm GaInNAsSb-SQW and 1.20 μm GaInAsSb-SQW ridge lasers," *Electron. Lett.*, vol. 36, pp. 1701–1703, Sept. 2000.

[10] V. Gambin, W. Ha, M. Wistey, H. Yuen, S. R. Bank, S. M. Kim, and J. S. Harris Jr., "GaInNAsSb for 1.3–1.6 μm long wavelength lasers grown by molecular beam epitaxy," *IEEE J. Select. Topics Quantum Electron.*, vol. 8, pp. 795–800, July–Aug. 2002.

[11] W. Ha, V. Gambin, S. Bank, M. Wistey, H. Yuen, S. Kim, and J. S. Harris Jr., "Long-wavelength GaInNAs(Sb) lasers on GaAs," *IEEE J. Quantum Electron.*, vol. 38, pp. 1260–1267, Sept. 2002.

[12] L. H. Li, V. Sallet, G. Patriarche, L. Largeau, S. Bouchoule, K. Merghem, L. Travers, and J. C. Harmand, "1.5 μm laser on GaAs with GaInNAsSb quinary quantum well," *Electron. Lett.*, vol. 39, pp. 519–520, Mar. 2003.

[13] S. R. Bank, M. A. Wistey, H. B. Yuen, L. L. Goddard, W. Ha, and J. S. Harris Jr., "Low-threshold CW GaInNAsSb/GaAs laser at 1.49 μm," *Electron. Lett.*, vol. 39, pp. 1445–1446, Oct. 2003.

[14] M. A. Wistey, S. R. Bank, H. B. Yuen, and J. S. Harris Jr., "Real-time measurement of GaInNAs nitrogen plasma ion flux," presented at the 2003 North American MBE Conf., Keystone, CO, p. 133.

[15] S. G. Spruytte, M. C. Larson, W. Wampler, C. W. Coldren, H. E. Peterson, and J. S. Harris, "Nitrogen incorporation in group III-nitride-arsenide materials grown by elemental source molecular beam epitaxy," *J. Cryst. Growth*, vol. 227–228, pp. 506–515, July 2001.

[16] N. Tansu, Y. L. Chang, T. Takeuchi, D. P. Bour, S. W. Corzing, M. R. T. Tan, and L. J. Mawst, "Temperature analysis and characteristics of highly strained InGaAs-GaAsP-GaAs ($\lambda > 1.17$ μm) quantum-well lasers," *IEEE J. Quantum Electron.*, vol. 38, pp. 640–651, June 2002.

[17] P. J. A. Thijs, "Strained-layer InGaAs(P)/InP quantum well semiconductor lasers grown by organometallic vapor phase epitaxy," Ph.D. dissertation, Technische Universiteit Delft, Delft, The Netherlands, 1994.

[18] H. B. Yuen, S. R. Bank, M. A. Wistey, W. Ha, V. Gambin, A. Moto, and J. S. Harris Jr., "Analysis of material properties of GaNAs(Sb) grown by MBE," presented at the 45th Electronic Materials Conf., Salt Lake City, UT, 2003, p. 88.

[19] A. Kaschner, T. Luttgert, H. Born, A. Hoffmann, A. Y. Egorov, and H. Riechert, "Recombination mechanisms in GaInNAs/GaAs multiple quantum wells," *Appl. Phys. Lett.*, vol. 78, pp. 1293–1391, Mar. 2001.

[20] A. Polimeni, M. Capizzi, M. Geddo, M. Fischer, M. Reinhardt, and A. Forchel, "Effect of temperature on the optical properties of (InGa)(AsN)/GaAs single quantum wells," *Appl. Phys Lett.*, vol. 77, pp. 2870–2872, Oct. 2000.

[21] M. A. Pinault and E. Tournie, "On the origin of carrier localization in $Ga_{1-x}In_xN_yAs_{1-y}/GaAs$ quantum wells," *Appl. Phys. Lett.*, vol. 78, pp. 1562–1564, Mar. 2001.

[22] J. Misiewicz, P. Sitarek, K. Ryczko, R. Kudrawiec, A. Fischer, M. Reinhardt, and A. Forchel, "Influence of nitrogen on carrier localization in InGaAsN/GaAs single quantum wells," *Microelectron. J.*, vol. 34, pp. 737–739, May–Aug. 2003.

[23] K. Volz, V. Gambin, W. Ha, M. A. Wistey, H. Yuen, S. Bank, and J. S. Harris, "The role of Sb in the MBE growth of (GaIn)(NAsSb)," *J. Cryst. Growth*, vol. 251, pp. 360–366, Apr. 2003.

[24] S. R. Bank, L. L. Goddard, M. A. Wistey, H. B. Yuen, and J. S. Harris Jr., "Effects of Auger recombination, carrier leakage, and intervalence band absorption in 1.5 μm GaInNAsSb lasers," *IEEE J. Quantum Electron*, to be published.

[25] L. L. Goddard, S. R. Bank, M. A. Wistey, H. B. Yuen, and J. S. Harris Jr., "Measurements of intrinsic properties of high power CW single quantum well GaInNAsSb/GaAs lasers at 1.5 μm," presented at the CLEO/QELS Conf., San Francisco, CA, 2004, p. 88.

[26] R. Fehse, S. Tomic, A. R. Adams, S. J. Sweeney, E. P. O'Reilly, A. Andreev, and H. Riechert, "A quantitative study of radiative, Auger, and defect related recombination processes in 1.3-μm GaInNAs-based quantum-well lasers," *IEEE J. Select. Topics Quantum Electron.*, vol. 8, pp. 801–810, July/Aug. 2002.

[27] E. P. O'Reilly and M. Silver, "Temperature sensitivity and high temperature operation of long wavelength semiconductor lasers," *Appl. Phys. Lett.*, vol. 63, pp. 3318–3320, Dec. 1993.

[28] T. Katsuyama, T. Yamada, Y. Iguchi, S. Takagishi, M. Murata, J. Hashimoto, and A. Ishida, "Very low threshold current GaInNAs quantum well lasers operating at 1.30 μm," presented at the *CLEO/QELS Conf.*, Baltimore, MD, 2003, p. 112.

[29] J. Piprek, *Semiconductor Optoelectronic Devices Introduction to Physics and Simulation*. San Diego, CA: Academic, 2003, p. 158.

[30] D. Gollub, S. Moses, M. Fischer, and A. Forchel, "1.42 μm continuous-wave operation of GaInNAs laser diodes," *Electron. Lett.*, vol. 39, pp. 777–778, May 2003.

[31] N. Tansu, J. Y. Yeh, and L. J. Mawst, "Low-threshold 1317-nm InGaAsN quantum-well lasers with GaAsN barriers," *Appl. Phys. Lett.*, vol. 83, pp. 2512–2514, Sept. 2003.

[32] R. Teissier, D. Sicault, J. C. Harmand, G. Ungaro, R. Le Roux, and L. Largeau, "Temperature-dependent valence band offset and band-gap energies of pseudomorphic GaAsSb on GaAs," *J. Appl. Phys.*, vol. 89, pp. 5473–5477, May 2001.

[33] N. Tansu and L. J. Mawst, "Low-threshold strain-compensated InGaAs(N) ($\lambda = 1.19 - 1.31$ μm) quantum-well lasers," *IEEE Photon. Technol. Lett.*, vol. 14, pp. 444–446, Apr. 2002.

[34] K. Prosyk, J. G. Simmons, and J. D. Evans, "Well number, length, and temperature dependence of efficiency and loss in InGaAsP–InP compressively strained MQW ridge waveguide lasers at 1.3 μm," *IEEE J. Quantum Electron.*, vol. 33, pp. 1360–1368, Aug. 1997.

[35] S. L. Chuang, *Physics of Optoelectronic Devices*. New York: Wiley, 1995.

[36] J. H. Angenent, M. Erman, J. M. Auger, R. Gamonal, and P. J. A. Thijs, "Extremely low loss InP/GaInAsP rib waveguides," *Electron. Lett.*, vol. 25, pp. 628–629, May 1989.

[37] N. N. Ledentsov, A. R. Kovsh, A. E. Zhukov, N. A. Maleev, S. S. Mikhrin, A. P. Vasil'ev, E. S. Semenova, M. V. Maximov, V. M. Ustinov, and D. Bimberg, "High performance quantum dot lasers on GaAs substrates operating in the 1.5 μm range," *Electron. Lett.*, vol. 39, pp. 1126–1128, July 2003.

[38] C. H. Henry, R. A. Logan, F. R. Merritt, and J. P. Luongo, "The effect of intervalence band absorption on the thermal behavior of InGaAsP lasers," *IEEE J. Quantum Electron.*, vol. QE-19, pp. 947–952, June 1983.

[39] G. N. Childs, S. Brand, and R. A. Abram, "Intervalence band absorption in semiconductor laser materials," *Semicond. Sci. Technol.*, vol. 1, pp. 116–120, Aug. 1986.

[40] S. L. Chuang, *Physics of Optoelectronic Devices*. New York: Wiley, 1995, pp. 434–435.

[41] P. J. A. Thijs, J. J. M. Binsma, L. F. Tiemeijer, and T. van Dongen, "Submilliamp threshold current (0.62 mA at 0°C) and high output power (220 mW) 1.5 μm tensile strained InGaAs single quantum well lasers," *Electron. Lett.*, vol. 28, pp. 829–830, Apr. 1992.

[42] W. B. Joyce and R. W. Dixon, "Thermal resistance of heterostructure lasers," *J. Appl. Phys.*, vol. 46, pp. 855–862, Feb. 1975.

[43] J. Piprek, *Semiconductor Optoelectronic Devices: Introduction to Physics and Simulation*. San Diego, CA: Academic, 2003, pp. 62–64.

[44] ——, *Semiconductor Optoelectronic Devices: Introduction to Physics and Simulation*. San Diego, CA: Academic, 2003, pp. 143–144.

[45] D. G. Mehuys, "High-power semiconductor lasers," in *Semiconductor Lasers II: Materials and Structures*, E. Kapon, Ed. San Diego, CA: Academic, 1999, pp. 261–262.

Seth R. Bank (S'95) received the B.S. degree from the University of Illinois at Urbana-Champaign (UIUC), Urbana, and the M.S. degree from Stanford University, Stanford, CA, both in electrical engineering. He is currently working towards the Ph.D. degree at Stanford University.

While at UIUC, he worked on fabrication of InGaP–GaAs and InGaAs–InP HBTs. His research currently focuses on MBE growth, fabrication, and device physics of long-wavelength VCSELs and high-power edge-emitting lasers in the GaInNAsSb–GaAs material system. He has coauthored over 25 papers and presentations.

Mr. Bank is a recipient of the Gerald L. Pearson Memorial Fellowship (Stanford) and the John Bardeen Scholarship (UIUC).

Mark A. Wistey (S'93) received the B.S. degree in electrical engineering from Montana State University-Bozeman. He received the M.S. degree from Stanford University, Stanford, CA, where he is currently working toward the Ph.D. degree.

His current research is on long-wavelength optoelectronics and VCSELs on GaAs, using dilute nitrides such as GaInNAs, grown by MBE. He is the coauthor of several papers and presentations related to dilute nitrides.

Lynford L. Goddard was born in Redwood City, CA, on June 10, 1975. He received the B.S. degree in math and physics and the M.S. degree in electrical engineering from Stanford University, Stanford, CA, in 1998 and 2003, respectively. His undergraduate honors thesis covered linear differential operators. He is currently working toward the Ph.D. degree in physics at Stanford University, where his research areas are GaInNAsSb–GaAs laser characterization and modeling.

At Xerox Palo Alto Research Center, he characterized the gain of 400-nm InGaN lasers during life testing.

Homan B. Yuen received the B.A. degree in physics from the University of California at Berkeley in 2000 and the M.S. degree in electrical engineering from Stanford University, Stanford, CA, in 2003. He is currently working toward the Ph.D. degree in materials science and engineering at Stanford University, studying the GaInNAsSb–GaAs material system for applications in long-wavelength optoelectronic devices.

Vincenzo Lordi received the B.S.E. degree in chemical engineering from Princeton University, Princeton, NJ, in 1999 and the M.S. degree in electrical engineering from Stanford University, Stanford, CA, in 2002. He is currently working toward the Ph.D. degree in materials science and engineering at Stanford, where his work is supported by a Fannie and John Hertz Foundation Fellowship.

While at Princeton, he studied the mechanical and chemical properties of carbon nanotubes using transmission electron microscopy and molecular dynamics simulations. His work included the synthesis of the first single-walled carbon nanotube supported metal catalyst. At Stanford, he is currently studying the GaInNAs(Sb)–GaAs material system for the realization of near-infrared optoelectronics, especially modulators, on GaAs, for telecommunications and optical interconnect applications.

James S. Harris, Jr., (S'66–M'68–SM'77–F'88) received the B.S., M.S. and Ph.D. degrees in electrical engineering from Stanford University, Stanford, CA, in 1964, 1965 and 1969, respectively.

He is currently the James and Ellenor Chesebrough Professor of Electrical Engineering, Applied Physics and Materials Science at Stanford University. In 1969, he joined the Rockwell International Science Center, Thousand Oaks, CA where he was one of the key contributors to ion implantation, MBE, and heterojunction devices, leading to their preeminent position in GaAs technology. In 1980, he became Director of the Optoelectronics Research Department and in 1982, he joined the Solid State Electronics Laboratory, Stanford University, as a Professor of electrical engineering. He served as Director of the Solid State Electronics Laboratory (1984–1998) and Director of the Joint Services Electronics Program (1985–1999). His current research interests are in the physics and application of ultrasmall structures and novel materials to new high-speed and spin-based electronic and optoelectronic devices and systems. He has supervised over 65 Ph.D. students, and has over 650 publications and 14 issued U.S. patents in these areas.

Dr. Harris is a Fellow of the American Physical Society. He received the 2000 IEEE Morris N. Liebmann Memorial Award, the 2000 International Compound Semiconductor Conference Welker Medal, an IEEE Third Millennium Medal, and an Alexander von Humboldt Senior Research Prize in 1998 for his contributions to GaAs devices and technology.